

Role of 53BP1 in end protection and DNA synthesis at DNA breaks

Jacob Paiano,^{1,7} Nicholas Zolnerowich,^{1,7} Wei Wu,¹ Raphael Pavani,¹ Chen Wang,^{2,6} Hongzhi Li,^{2,3} Li Zheng,^{2,3} Binghui Shen,^{2,3} Barry P. Sleckman,^{4,5} Bo-Ruei Chen,^{4,5} and André Nussenzweig¹

¹Laboratory of Genome Integrity, National Cancer Institute, National Institutes of Health, Bethesda, Maryland 20892, USA;

²Department of Cancer Genetics and Epigenetics, ³Department of Molecular Medicine, Beckman Research Institute of City of Hope, Duarte, California 91010, USA; ⁴Division of Hematology and Oncology, ⁵O'Neal Comprehensive Cancer Center, University of Alabama at Birmingham, Birmingham, Alabama 35294, USA

Double-strand break (DSB) repair choice is greatly influenced by the initial processing of DNA ends. 53BP1 limits the formation of recombinogenic single-strand DNA (ssDNA) in BRCA1-deficient cells, leading to defects in homologous recombination (HR). However, the exact mechanisms by which 53BP1 inhibits DSB resection remain unclear. Previous studies have identified two potential pathways: protection against DNA2/EXO1 exonucleases presumably through the Shieldin (SHLD) complex binding to ssDNA, and localized DNA synthesis through the CTC1-STN1-TEN1 (CST) and DNA polymerase α (Pola) to counteract resection. Using a combinatorial approach of END-seq, SAR-seq, and RPA ChIP-seq, we directly assessed the extent of resection, DNA synthesis, and ssDNA, respectively, at restriction enzyme-induced DSBs. We show that, in the presence of 53BP1, Pola-dependent DNA synthesis reduces the fraction of resected DSBs and the resection lengths in G0/G1, supporting a previous model that fill-in synthesis can limit the extent of resection. However, in the absence of 53BP1, Pola activity is sustained on ssDNA yet does not substantially counter resection. In contrast, EXO1 nuclease activity is essential for hyperresection in the absence of 53BP1. Thus, Pola-mediated fill-in partially limits resection in the presence of 53BP1 but cannot counter extensive hyperresection due to the loss of 53BP1 exonuclease blockade. These data provide the first nucleotide mapping of DNA synthesis at resected DSBs and provide insight into the relationship between fill-in polymerases and resection exonucleases.

[*Keywords:* 53BP1; end resection; homologous recombination]

Supplemental material is available for this article.

Received May 14, 2021; revised version accepted August 17, 2021.

Double-strand break (DSB) repair is accomplished by two primary mechanisms: nonhomologous end joining (NHEJ) and homology-directed repair (HDR). NHEJ is faster, more error-prone, and occurs in all phases of the cell cycle but is the primary pathway of DSB repair in G1 (Karanam et al. 2012; Zhao et al. 2020). HDR predominates in S phase, is usually error-free owing to the use of a donor sequence, and requires end resection for annealing DSB ends to the donor template for repair. The key factor that dictates how cells choose between NHEJ and HDR is the extent of single-strand DNA (ssDNA) at the break site, with an increasing amount needed to expose homology for repair by HDR. End resection is promoted by BRCA1, possibly by antagonizing 53BP1, which limits the formation of ssDNA at DSBs (Bouwman et al. 2010; Bunting et al. 2010). While loss of 53BP1 results in hyperresection and

long 3' overhangs, the mechanism by which 53BP1 inhibits resection remains unclear. Two models have been proposed: The first is that 53BP1 directly shields DNA from exonucleases, and the second is that resection is counteracted through fill-in by DNA synthesis (Setiapatra and Durocher 2019; Mirman and de Lange 2020).

Both models are thought to require 53BP1 effectors, including RIF1, Shieldin (REV7, SHLD1-SHLD2-SHLD3), and the CTC1-STN1-TEN1 (CST) complex. Loss of RIF1, Shieldin, or CST leads to increased ssDNA and RPA loading, decreased sensitivity to PARP inhibitor (PARPi) in BRCA1-deficient cells, impaired NHEJ at dysfunctional telomeres, and defective immunoglobulin class switch recombination (Chapman et al. 2013; Di Virgilio et al. 2013; Escribano-Díaz et al. 2013; Feng et al. 2013; Zimmermann et al. 2013; Barazas et al. 2018; Dev

⁶Present address: The Wistar Institute, University City, Philadelphia, PA 19104, USA.

⁷These authors contributed equally to this work.

Corresponding author: andre_nussenzweig@nih.gov

Article published online ahead of print. Article and publication date are online at <http://www.genesdev.org/cgi/doi/10.1101/gad.348667.121>.

© 2021 Paiano et al. This article is distributed exclusively by Cold Spring Harbor Laboratory Press for the first six months after the full-issue publication date (see <http://genesdev.cshlp.org/site/misc/terms.xhtml>). After six months, it is available under a Creative Commons License (Attribution-NonCommercial 4.0 International), as described at <http://creativecommons.org/licenses/by-nc/4.0/>.

et al. 2018; Findlay et al. 2018; Gao et al. 2018; Ghezraoui et al. 2018; Gupta et al. 2018; Mirman et al. 2018; Noor-dermeer et al. 2018; Tomida et al. 2018; Mirman and de Lange 2020). According to the first model, Shieldin directly inhibits exonuclease activity by physically blocking the free DNA ends. Shld2 directly binds ssDNA *in vitro* via OB folds analogous to RPA (Dev et al. 2018; Findlay et al. 2018; Gao et al. 2018). Shieldin may therefore block EXO1- or DNA2-mediated exonucleolytic resection by competing with RPA, as RPA has been shown to stimulate resection exonucleases (Cejka et al. 2010; Soniat et al. 2019). In addition, Shieldin recruits CST, which also forms a ssDNA binding complex containing multiple OB fold domains (Miyake et al. 2009), which may in turn inhibit resection nucleases. In contrast, the second model posits that the activity of CST/Pola/primase counteracts resection via Pola-dependent DNA synthesis (Mirman et al. 2018). It has been shown that CST/Pola/primase acts downstream from Shieldin, that CST depletion or Pola inhibition leads to PARPi resistance in BRCA1-deficient cells, and that CST acts in an epistatic manner with Pola (Barazas et al. 2018; Mirman et al. 2018). This suggests CST-Pola counter hyperresection downstream from 53BP1, likely by Pola-dependent DNA synthesis (Mirman et al. 2018).

Here, we address the interplay of these two distinct modes of 53BP1 action at DSBs by directly examining and quantifying the levels of ssDNA and DNA synthesis at restriction enzyme-induced DSBs through next-generation sequencing. We found that, in the presence of 53BP1, Pola-dependent synthesis counteracts resection at DSBs. When Pola is inhibited, resection is increased and synthe-

sis around the break is decreased. However, in the absence of 53BP1, Pola is surprisingly still active at DSBs but is unable to counteract hyperresection of DNA ends. This suggests that the end protection function of 53BP1 is likely to be the predominant mechanism by which it blocks end resection.

Results

Mapping resection and DNA synthesis at DNA breaks

We have shown that END-seq, a method that directly maps DSBs, and RPA single-strand DNA sequencing (SSDS) can be used to determine the extent of 5' end resection (Khil et al. 2012; Canela et al. 2016; Tubbs et al. 2018; Callen et al. 2020; Paiano et al. 2020). Additionally, we recently developed a next-generation sequencing method to map DNA synthesis associated with repair (SAR-seq) that can accurately map DNA polymerase activity at sites of damage in nondividing cells (Wu et al. 2021). To directly test the extent to which 53BP1 mediates localized fill-in DNA synthesis at DSBs, we used a combinatorial sequencing strategy that measures resection (by END-seq and RPA SSDS) and DNA polymerase activity (by SAR-seq) in murine *v-abl* kinase transformed pre-B cells harboring AsiSI-induced DSBs (Iacovoni et al. 2010; Canela et al. 2016). Cells were arrested in G0/G1 phase using the *v-abl* kinase inhibitor imatinib, followed by doxycycline (DOX)-induced expression of AsiSI fused to estrogen receptor (ER), and then nuclear translocation of AsiSI-ER by 4-hydroxytamoxifen (4-OHT) for 18 h (Fig. 1A; Canela et al. 2016). Most cells (90%) were viable and

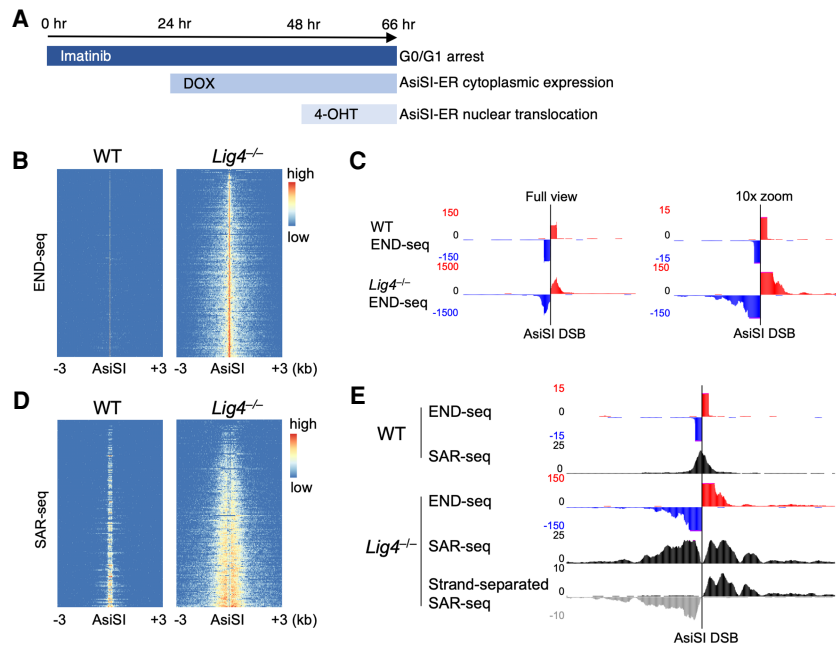


Figure 1. Resected 3' overhangs undergo extensive DNA synthesis. (A) Inducing AsiSI restriction enzyme breaks in Abelson-transformed murine pre-B cells. Cycling cells were arrested in G0/G1 for 24 h with the Abelson kinase inhibitor imatinib, followed by 24 h of doxycycline (DOX) to express AsiSI fused to estrogen receptor (AsiSI-ER). Double-strand breaks were synchronously induced by 4-hydroxytamoxifen (4-OHT) that translocated AsiSI-ER into the nucleus. (B) Heat maps of END-seq signal ± 3 kb around the strongest (i.e., the most significant and reproducible) 200 AsiSI cut sites, ordered by total read count, for WT and *Lig4*^{-/-} cells after 18 h AsiSI induction in which extensive resection is observed in *Lig4*^{-/-}. (C) Genome browser snapshot of strand-separated END-seq reads at a single AsiSI location (chr9: 121,477,509–121,477,517), either at full view in Y-axis read intensity (left) or zoomed in 10-fold (right) to better view distal resection reads. (Red) Positive strand, (blue) negative strand. (D) Heat maps of localized DNA synthesis as detected by SAR-seq ± 3 kb around AsiSI cut sites in WT and *Lig4*^{-/-} cells after 18 h AsiSI induction. (E) Genome browser snapshot of WT and *Lig4*^{-/-} cells showing END-seq and SAR-seq at a single AsiSI location (chr9: 121,477,509–121,477,517). (Bottom) A modification to the SAR-seq protocol in which only EdU-incorporated DNA strands are sequenced (“strand-separated SAR-seq”) shows that DNA synthesis occurs exclusively on resected 3' overhangs. All panels show representative data sets from two independent replicate experiments.

G0/G1-arrested before and after 18-h 4-OHT treatment, and all cells were confirmed to be *Lig4*-KO by PCR (Supplemental Fig. S1A,B). AsiSI cutting was evident in >90% of cells as determined by flow cytometry using the DSB marker phosphorylated KAP1, confirming that most cells experience DSBs (Supplemental Fig. S1B). After 18 h of AsiSI cutting, little to no resection was detected by END-seq in WT cells; however, all DSBs exhibited significant resection in DNA ligase 4-deficient (*Lig4*^{-/-}) cells in which NHEJ is blocked, although most breaks (~80%) (Fig. 2D) still remained unresected (Fig. 1B,C). Sequencing reads from both sides of the break align unambiguously to either the positive or negative DNA strand, indicating a single AsiSI cut site and resected overhangs that are purely 3' in nature (Fig. 1C; Supplemental Fig. S1C; Paiano et al. 2020). Consistent with these findings, 5' end resection was observed at dysfunctional telomeres in MEFs lacking LIG4 (Mirman et al. 2018).

Strikingly, we detected robust DNA synthesis at AsiSI breaks by SAR-seq, in which the thymidine analog EdU is added to cells simultaneously with 4-OHT, after which EdU-incorporated DNA is enriched and processed for sequencing (Fig. 1D; Wu et al. 2021). While WT cells exhibited a single, sharp SAR-seq peak directly at the DSB, likely indicating NHEJ polymerase activity during repair, *Lig4*^{-/-} cells showed extensive SAR-seq signal distal to the break sites (Fig. 1D,E; Supplemental Fig. S1D). Moreover, in *Lig4*^{-/-} cells, the read distribution of SAR-seq and END-seq overlapped extensively, demonstrating

that breaks genome-wide undergo localized DNA synthesis on resected 3' ssDNA overhangs (Supplemental Fig. S1E). This was further supported by performing a modified, DNA strand-separated SAR-seq in which only EdU-incorporated DNA strands were PCR-amplified and sequenced (Wu et al. 2021). Before PCR amplification, EdU-enriched dsDNA fragments captured on streptavidin beads were briefly denatured by NaOH, and non-EdU strands were washed away, so that only EdU-containing ssDNA fragments were sequenced (Supplemental Fig. S1F). While SAR-seq typically does not provide DNA strand information, strand-separated SAR-seq revealed that DNA was exclusively synthesized on 3' overhangs generated by resection (Fig. 1E; Supplemental Fig. S1D, G). Because WT cells showed virtually no resection under these conditions (Canela et al. 2016; Mirman and de Lange 2020), we performed all subsequent studies using *Lig4*^{-/-} cells in which measurable resection occurs.

DNA synthesis counters the extent of resection

The high prevalence of DNA synthesis on resected DSB ends prompted us to ask whether this synthesis is directly involved in countering the resection machinery, as has been recently suggested (Mirman et al. 2018). Consistently, we found that concurrent treatment with the B family DNA polymerase inhibitor, aphidicolin (APH), significantly increased the fraction of resected DSBs (Fig. 2A). This was further supported by the increase in RPA-bound

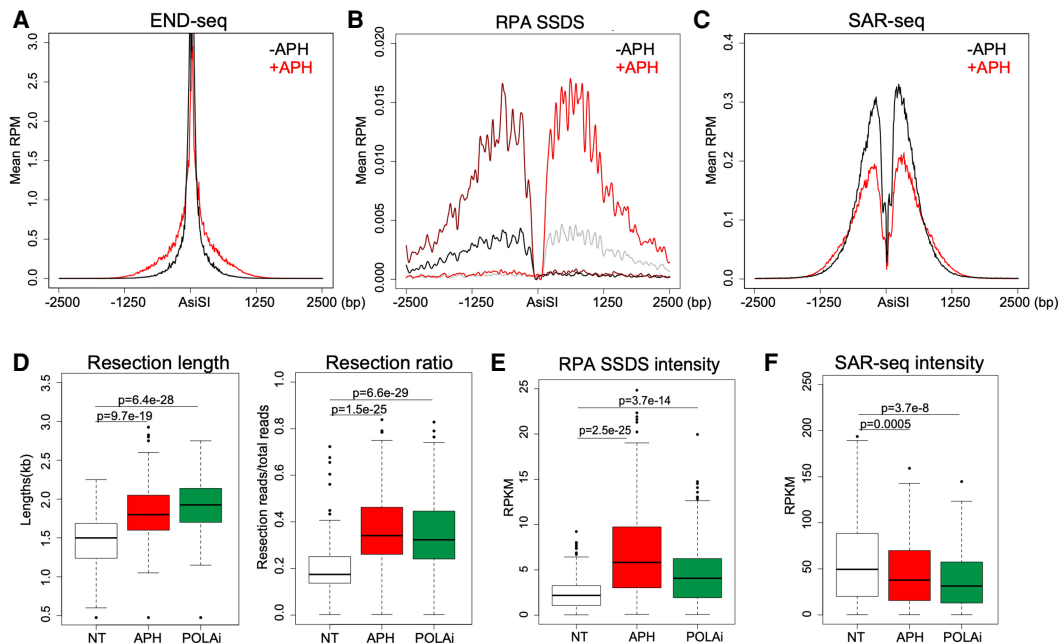


Figure 2. Decreased DNA synthesis or Pol α /primase activity increases resection. (A–C) Average reads per million (RPM) aggregated ± 2.5 kb around the strongest 200 AsiSI break sites of END-seq (A), RPA ssDNA sequencing (SSDS) (B), and SAR-seq (C) in *Lig4*^{-/-} pre-B cells treated with or without 5 μ M aphidicolin (APH) during AsiSI cutting. (D) Box plots of calculated resection lengths (left) and ratio of resected breaks versus total breaks (right) as detected by END-seq. Each data point represents a specific AsiSI genomic location. AsiSI cutting was induced in *Lig4*^{-/-} cells with either no additional treatment (NT), 5 μ M APH, or 1 μ M DNA Pol α inhibitor (POLAi) concurrent treatment. (E,F) Box plots of signal intensity for RPA SSDS (E) and SAR-seq (F) in *Lig4*^{-/-} cells after AsiSI induction with either NT, 5 μ M APH, or 1 μ M POLAi concurrent treatment. All panels show representative data sets from two independent replicate experiments.

ssDNA surrounding AsiSI sites genome-wide (Fig. 2B). These data strongly suggest that inhibition of DNA synthesis in G0/G1 cells promotes exonuclease activity at DSBs. Another nonexclusive possibility is that inhibiting POL α -driven DNA synthesis exposes more ssDNA for RPA loading.

SAR-seq revealed a significant, though incomplete, reduction of fill-in polymerase activity around AsiSI sites in the presence of 5 μ M APH, suggesting that, at this dose, DNA synthesis is likely delayed but not fully inhibited, which still allows for increased resection activity by slowing DNA polymerases (Fig. 2C). At a higher dose (50 μ M), DNA synthesis was further blocked, while resection increased slightly compared with 5 μ M APH treatment (Supplemental Fig. S2A,B). Similar results were obtained by treating cells with the ribonucleotide reductase inhibitor hydroxyurea, in which resection increased by both END-seq and RPA SSSDs, while SAR-seq was significantly reduced (Supplemental Fig. S2C–E).

DNA synthesis on resected ends is polymerase α -dependent

It has been suggested that Pola, in association with CST, 53BP1, and Shieldin, is recruited to sites of DNA damage (Mirman et al. 2018). To test the role of Pola in counteracting resection, we treated cells with the Pola inhibitor adarotene during AsiSI cutting (Abdel-Samad et al. 2018; Cincinelli et al. 2020). We found increased resection lengths and resected DSB numbers by END-seq and RPA SSSDs upon Pola inhibition (Fig. 2D,E), which concomitantly decreased SAR-seq signal genome-wide (Fig. 2F). Similar results were obtained with an independent Pola inhibitor CD437 (Supplemental Fig. S2F). This strongly suggests that Pola activity is critical for synthesis at re-

sected DSBs and supports a previously proposed model in which Pola-mediated DNA synthesis regularly occurs at resected DSBs in G0/G1 to counter the extent of resection exonucleases (Supplemental Fig. S2G; Mirman et al. 2018).

DSB end fill-in is most consequential in G1 phase

End resection is essential in S phase when sister chromatids are available for repair by HDR. We therefore assayed resection in asynchronously cycling cells (comprising >70% S-phase cells) (Supplemental Fig. S1A) and G2-arrested cells. Cells were G2-arrested with 10 μ M RO3306 CDK1 inhibitor for 36 h and treated with DOX for the last 24 h for AsiSI-ER expression. 4-OHT was given for an additional 6 h to induce AsiSI cutting in G2 cells, which were viable and G2-arrested as confirmed by FACS profiling (~80% G2) (Supplemental Fig. S3). Interestingly, we found that, in WT cells, resection was detectable in asynchronously cycling cultures but was severely limited in G2, consistent with the finding that HDR is more prominent in S phase whereas NHEJ is the dominant repair pathway in G1 and G2 (Fig. 3A; Karanam et al. 2012). Indeed, resection in G2-arrested WT cells was more similar to that in G0/G1 resection than in S phase (Fig. 3A). Relative to WT cells, end resection was increased in G0/G1, S, and G2 phases in *Lig4*^{-/-} cells, suggesting that NHEJ is active and prevents resection throughout the cell cycle by allowing rapid end joining of DSB ends (Fig. 3A). Inhibiting DNA synthesis by APH did not significantly increase resection in both WT and *Lig4*^{-/-} asynchronous cells, indicating that fill-in is not a major factor that counters resection when broken sister chromatids are present (Fig. 3A,B). Moreover, resection did not substantially increase upon APH treatment in

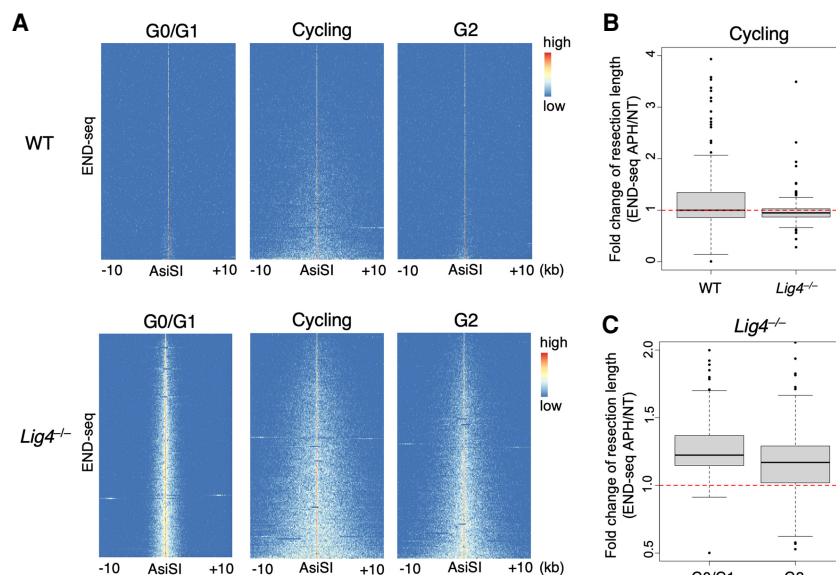


Figure 3. Resection and fill-in during S and G2 phases. (A) Heat maps of END-seq signal ± 10 kb from the strongest 200 AsiSI breaks in either WT (top row) or *Lig4*^{-/-} (bottom row) pre-B cells. Prior to AsiSI cutting, cells were either arrested in G0/G1 with imatinib (left), not arrested and remained asynchronously cycling (middle), or arrested in G2 with CDK1 inhibition. AsiSI was induced for 18 h in G0/G1 cells and 6 h in cycling and G2 cells. Extensive resection (>5 kb) is observed only in cycling/S-phase cells or in G2 when NHEJ is prevented (i.e., *LIG4* deficiency). (B) Cycling WT or *Lig4*^{-/-} pre-B cells were treated with 5 μ M aphidicolin (APH) or no additional treatment (NT) during 6-h AsiSI cutting. Box plots represent the fold change in maximum resection length per break in APH over NT conditions. (C) Box plots of the ratio of APH to NT maximum resection length per break in *Lig4*^{-/-} pre-B cells arrested in either G0/G1 or G2 measured by END-seq. While resection robustly increases in G0/G1 with APH treatment, a modest increase is observed in G2. All panels show data sets from one experiment.

resection robustly increases in G0/G1 with APH treatment, a modest increase is observed in G2. All panels show data sets from one experiment.

LIG4-deficient cells arrested in G2 (Fig. 3C), suggesting that fill-in may be most significant in limiting resection at restriction enzyme-induced DSBs in G0/G1.

Polymerase α /primase priming is necessary for fill-in synthesis

To further confirm Pola activity on resected 3' overhangs, we developed a modification to SAR-seq to assay for in vivo Pola/primase DNA primers. We hypothesized that if Pola/primase-mediated template primers were present on 3' overhangs alongside ssDNA gaps yet to be filled in, recombinant DNA polymerases added in vitro should be able to synthesize DNA starting from the 3' dsDNA primer end. If such primers did not exist, then recombinant polymerases would be unable to synthesize any DNA on the resected 3' overhang. In this adapted "in vitro SAR-seq"

method, live cells were not incubated with EdU. Rather, after AsiSI induction and drug treatment, cells were harvested and embedded live in agarose plugs. After overnight proteinase K treatment, plugs harboring resected DSB ends underwent an in situ synthesis reaction with one of three DNA polymerases (DNA polymerase I, Klenow fragment 3' \rightarrow 5' exo $^{-}$, or T4 DNA polymerase) in the presence of dATP, dGTP, dCTP, and EdU (in place of dTTP). Plugs were then melted, DNA was sonicated, and EdU fragments were biotin-labeled and enriched per the SAR-seq protocol (Wu et al. 2021). After 18 h AsiSI induction in *Lig4* $^{-/-}$ cells, in vitro SAR-seq did not detect any EdU incorporation, suggesting that no unligated DNA primers were present, likely due to the completion of fill-in synthesis (Fig. 4A). However, if cells were treated with APH for 18 h during AsiSI cutting, EdU was incorporated at DSBs by in vitro SAR-seq (Fig. 4B). APH has been

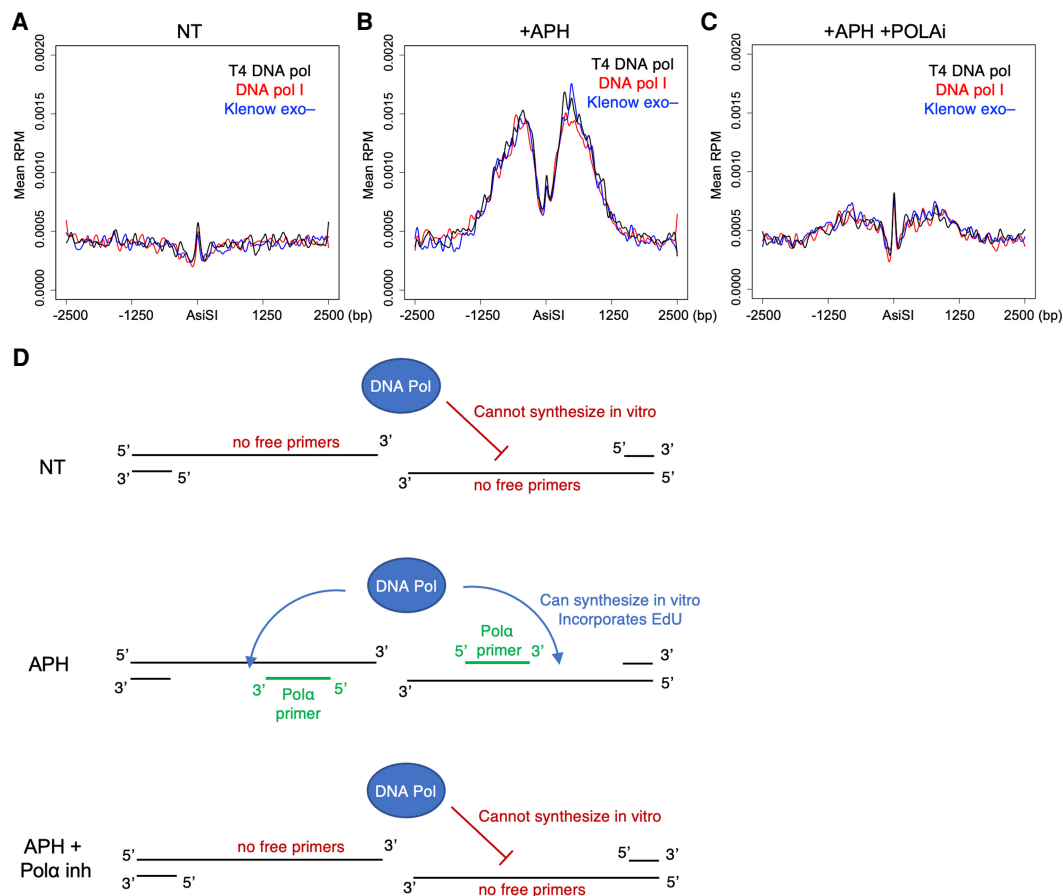


Figure 4. In vitro SAR-seq demonstrates the presence of Pola/primase primers on resected ends. (A–C) Aggregated reads per million (RPM), averaged across the strongest 200 AsiSI breaks, of in vitro SAR-seq signal ± 2.5 kb around AsiSI sites. Eighteen-hour AsiSI-induced *Lig4* $^{-/-}$ cells were given either no additional treatment (NT) (A), 5 μ M aphidicolin (APH) (B), or 5 μ M APH and 1 μ M DNA Pola inhibitor (POLAi) (C). In vitro synthesis reactions were performed using either recombinant DNA polymerase I (red), T4 DNA polymerase (black), or Klenow fragment exo $^{-}$ (blue). (D, top) In vitro SAR-seq signal was only detected with APH, as NT conditions likely did not retain any free DNA primers and open ssDNA gaps to initiate and elongate in vitro synthesis reactions. (Middle) During polymerase inhibition in the presence of APH, primers and gaps likely exist at the time of cell capture, allowing for recombinant DNA polymerases to incorporate EdU onto 3' overhangs that is then enriched and sequenced by SAR-seq. (Bottom) The abolished in vitro SAR-seq signal observed during APH + POLAi treatments confirms that these primers are laid by Pola/primase in vivo. Panels show representative data sets from two independent replicate experiments.

shown *in vitro* to leave Pola priming intact (Sheaff et al. 1991); therefore, these data suggest that APH slows *in vivo* polymerase activity such that primers exhibit significant ssDNA gaps that could be filled in. *In vitro* SAR-seq signal was abolished if cells were treated with Pola inhibitor in addition to APH during AsiSI induction, thereby confirming Pola as the protein responsible for priming synthesis on resected DSB ends (Fig. 4C). These data indicate that Pola priming and fill-in typically happen quickly without leaving persistent ssDNA gaps. The addition of APH slows Pola such that synthesis still occurs, yet ssDNA gaps are present along the 3' overhang (Fig. 4D).

Polymerase α activity is 53BP1-independent

In cells lacking LIG4 and TRF2, telomere resection is exacerbated by loss of 53BP1 or CST (Mirman et al. 2018). To examine the interplay of end resection and DNA synthesis in cells lacking 53BP1, we performed END-seq, RPA SSSS, and SAR-seq on *Lig4*^{-/-} AsiS-ER pre-B cells after knocking out 53BP1 (*Lig4*^{-/-}*53bp1*^{-/-}) (Supplemental Figs. S1B, S4A,B). As expected, hyperresection was observed by END-seq at all resected AsiSI DSBs after loss of 53BP1 (Fig. 5A,B; Supplemental Fig. S4C; Canela et al. 2016).

To test whether hyperresection was due to increased initiation of resection, we performed MRE11 ChIP-seq and found similar levels of MRE11 at AsiSI breaks in *Lig4*^{-/-} and *Lig4*^{-/-}*53bp1*^{-/-} cells, suggesting increased long-range resection rather than increased MRE11 initiation (Supplemental Fig. S4D). In contrast to *Lig4*^{-/-} cells in which APH or Pola inhibitor roughly doubled resected DSBs (~20% to ~40% resected ends) (Fig. 2D), inhibition of DNA synthesis, by either APH or Pola inhibitor, did not robustly increase resected DSBs or resection track lengths in *Lig4*^{-/-}*53bp1*^{-/-} cells (Fig. 5C). Indeed, in *Lig4*^{-/-}*53bp1*^{-/-} cells, ~60% of DSBs were resected regardless of DNA polymerase inhibition (Fig. 5C). This was further confirmed by RPA SSSS, in which the amount of RPA-bound ssDNA did not robustly change with inhibitor treatments, compared with the same treatments in *Lig4*^{-/-} cells (Figs. 2E, 5D; Supplemental Fig. S4E). Similar results were obtained using an independently derived *Lig4*^{-/-}*53bp1*^{-/-} clone for all experiments (Supplemental Fig. S5). These data suggest that either Pola fill-in does not occur in the absence of 53BP1 or that Pola fill-in does occur but cannot counter extensive hyperresection due to loss of 53BP1 exonuclease blockade.

To test this, we performed SAR-seq on *Lig4*^{-/-} versus *Lig4*^{-/-}*53bp1*^{-/-} cells after 18-h AsiSI induction. In the absence of 53BP1, substantial DNA synthesis was still detected along resected DNA ends (Fig. 5E,F; Supplemental Fig. S5E,F). SAR-seq read intensity per AsiSI locus (i.e., the level of sequenced EdU-incorporated DNA per DSB location) was very similar between *Lig4*^{-/-} and *Lig4*^{-/-}*53bp1*^{-/-} cells, demonstrating that DNA synthesis was unaffected by the loss of 53BP1 (Fig. 5G; Supplemental Fig. S5G). Importantly, we found that this DNA synthesis was also dependent on Pola (Fig. 5H; Supple-

mental Fig. 5H). We therefore favor a model in which Pola can be recruited to resected DSB ends independently of 53BP1 and can limit the overall extent of resection by exonucleases through fill-in synthesis. In the absence of 53BP1, resection occurs more frequently and at greater lengths, a phenotype that is independent of Pola activity and instead likely occurs due to loss of end protection (Supplemental Fig. 4F).

To examine the role of shieldin complex in limiting resection, we generated *Lig4*^{-/-}*Rev7*^{-/-} pre-B cells (Supplemental Fig. S6A) and performed END-seq and SAR-seq after AsiSI induction. We found substantial fill-in synthesis present at DSBs in *Lig4*^{-/-}*Rev7*^{-/-} pre-B cells (Supplemental Fig. S6B). This synthesis was significantly reduced with APH and POLAi, suggesting POLA-dependent fill-in mechanisms similar to what we observed in *Lig4*^{-/-}*53bp1*^{-/-} cells (Supplemental Fig. S6B). Together, these data support a model in which 53BP1/Shieldin limit resection primarily through end protection in G1 cells.

53bp1-null hyperresection depends primarily on EXO1 nuclease activity

If 53BP1 limits resection through Shieldin-mediated end protection, loss of end processing should rescue the hyperresection observed in *Lig4*^{-/-}*53bp1*^{-/-} cells. We therefore tested the roles of 5'-3' exonucleases DNA2 and EXO1 to carry out resection in the absence of 53BP1. To do so, we treated cells with specific inhibitors against either DNA2 or EXO1 during AsiSI cutting and measured resection track lengths by END-seq. We identified a novel EXO1 inhibitor (EXO1i), C73, from a virtual screen of a library of >260,000 compounds of predicted druggable sites based on the human EXO1 X-ray structure (Supplemental Fig. S7A,B). We found C73 to be a potent and selective *in vitro* inhibitor of EXO1 activity by both a fluorescence resonance energy transfer (FRET)-based exonuclease assay and a ³²P-based exonuclease assay (Supplemental Fig. S7C-F). We validated the efficacies of the DNA2 inhibitor (DNA2i) and EXO1i by quantifying RPA foci in WT and *Brcal* ^{Δ 11/ Δ 11}*53bp1*^{-/-} mouse embryonic fibroblasts (MEFs) after 10 Gy γ irradiation, in which combination of both inhibitors diminished RPA loading as expected (Supplemental Fig. S7G; Symington 2016).

In G0/G1-arrested *Lig4*^{-/-} cells, we found resection to be entirely dependent on EXO1 activity, as our EXO1i abolished most resection signal by END-seq, whereas DNA2i had no effect (Fig. 5I). Interestingly, in *Lig4*^{-/-}*53bp1*^{-/-} cells, inhibition of DNA2 decreased maximum hyperresection lengths while EXO1i almost entirely eliminated the signal (Fig. 5J). These data suggest that 53BP1/Shieldin mediate end protection to prevent hyperresection by limiting the activity of both DNA2 and EXO1, although selective blocking against DNA2 may be more critical to limiting very long, hyperresected tracks in G1 (Fig. 5I,J). Thus, although DNA2 and EXO1 are generally thought to act redundantly to reveal 3' single-stranded tails (Symington 2016), they appear to play distinct roles in removing short versus long tracts in our system.

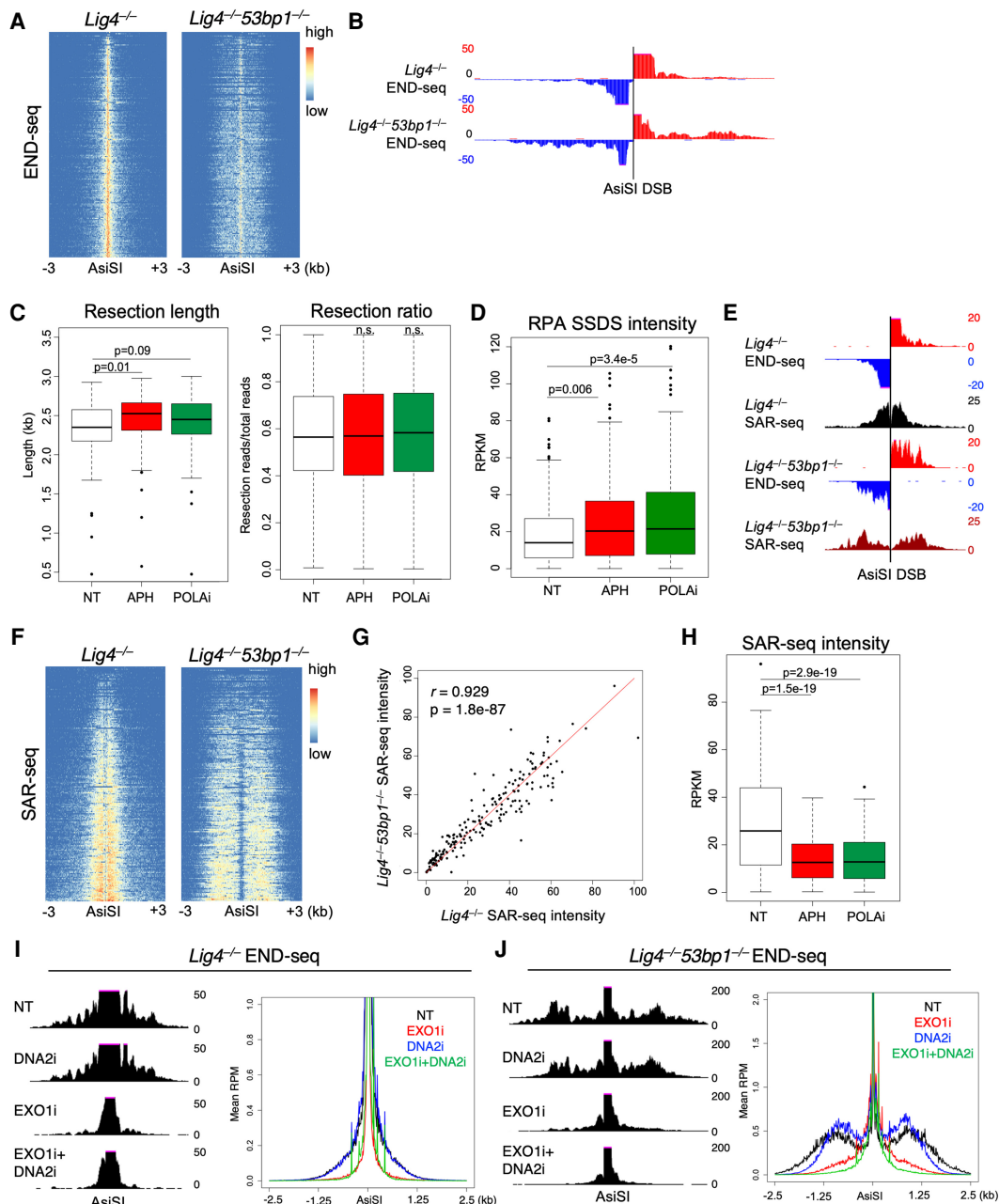


Figure 5. Pola/primase activity in the absence of 53BP1 does not limit EXO1-dependent hyperresection. (**A**) Heat maps of END-seq signal ± 3 kb around the top 200 AsiSI breaks in *Lig4*^{-/-} and *Lig4*^{-/-53bp1}^{-/-} pre-B cells after 18-h AsiSI cutting. (**B**) Genome browser snapshot of DNA strand-separated END-seq in *Lig4*^{-/-} and *Lig4*^{-/-53bp1}^{-/-} cells at a single AsiSI break (chr12: 111,039,088–111,039,096). More reads distal to AsiSI sites in *Lig4*^{-/-53bp1}^{-/-} compared with *Lig4*^{-/-} indicates increased numbers and track lengths of resected breaks, consistent with the expected hyperresection phenotype. (**C**) Box plots of maximum resection lengths per AsiSI site (left) and ratio of resected breaks versus total breaks (right) as detected by END-seq after AsiSI induction with either no additional treatment, 5 μ M aphidicolin (APH), or 1 μ M DNA Pola inhibitor (POLAi) concurrent treatment. (**D**) Box plots of RPA single-strand DNA sequencing (SSDS) intensity in *Lig4*^{-/-53bp1}^{-/-} cells after 18-h AsiSI cutting with either NT, 5 μ M APH, or 1 μ M POLAi concurrent treatment. (**E**) Genome browser snapshot of SAR-seq signal at an individual AsiSI DSB with END-seq resection as reference (chr5: 115,630,000–115-635,000). (**F**) Heat maps of SAR-seq signal ± 3 kb around AsiSI sites in *Lig4*^{-/-} and *Lig4*^{-/-53bp1}^{-/-} cells after 18-h break induction. (**G**) Pearson's correlation of normalized read intensity at each AsiSI break location between *Lig4*^{-/-} and *Lig4*^{-/-53bp1}^{-/-} SAR-seq from **F**. (**H**) Box plots of SAR-seq intensity in *Lig4*^{-/-53bp1}^{-/-} cells after 18-h AsiSI cutting with either NT, 5 μ M APH, or 1 μ M POLAi concurrent treatment. (**I, J**) Eighteen-hour AsiSI END-seq on either *Lig4*^{-/-} (**I**) or *Lig4*^{-/-53bp1}^{-/-} (**J**) cells concurrently treated with DNA2 inhibitor (DNA2i), EXO1 inhibitor (EXO1i or C73), both, or NT. Resection signal at an individual AsiSI DSB (left, chr9: 63,756,000–63,761,000) and total resection signal aggregated and plotted for all 200 DSBs (right, Y-axis magnified to better visualize resection) are shown. All panels (except **I** and **J**, in which two independent replicate experiments were performed) show data sets from one experiment. **A–H** were independently corroborated using a separate *Lig4*^{-/-53bp1}^{-/-} clone in Supplemental Figure S5.

Discussion

Using a combinatorial approach of END-seq, SAR-seq, and RPA SSSDs, we show here the ability to characterize at nucleotide resolution the *in vivo* molecular events that regulate DSB resection. Both END-seq and RPA SSSDs precisely map the fraction and extent of resection by sequencing dsDNA-ssDNA junctions or RPA-bound ssDNA, respectively (Canela et al. 2016). To effectively study the molecular events of end resection *in vivo*, we initially used *Lig4*^{-/-} pre-B cells arrested in G0/G1 that are programmed to synchronously induce AsiSI breaks across the genome (Canela et al. 2016). These nondividing, NHEJ-deficient cells exhibit significant resection of AsiSI DSBs over time that are easily measured without the confounding effects of DNA replication forks or variable CDK activities present in cycling cell populations (Ferretti et al. 2013). By incubating cells with EdU over the course of AsiSI breakage, we detected by SAR-seq robust DNA synthesis localized on resected 3' overhangs. In *Lig4*^{-/-} cells, this synthesis was observed >1 kb from the DSB and correlated with resection tracks lengths measured by END-seq (Supplemental Fig. S1E). These data provide the first nucleotide mapping of *in vivo* DNA synthesis at resected DSBs and demonstrate a tractable experimental system to test potential interactions of fill-in polymerases and resection exonucleases.

We present evidence here that localized DNA synthesis, initiated by Pola/primase, can limit the fraction of resected DSB ends and resection lengths of DSBs in G0/G1. Broadly inhibiting synthesis using APH or hydroxyurea, or specifically inhibiting Pola, led to an increase in the number of resected DSBs and maximum resection track lengths. Our adaptation to SAR-seq, *in vitro* SAR-seq, that maps recombinant polymerase *in vitro* activity on suitable ssDNA substrates, further supports the localized activity of Pola at resected ends. In summary, we conclude that Pola acts upon resected 3' ends for fill-in synthesis and can counter resection exonuclease activity. Nevertheless, extensive ssDNA tracks are detectable even with intact Pola priming. Therefore, exonucleases are still able to generate significant, and ostensibly stable, ssDNA regardless of localized DNA synthesis.

Fill-in synthesis at two-ended DSBs is most prominent in G0/G1, when resection is limited. It has been reported that unrepaired AsiSI breaks cluster in G1 in a manner dependent on the resection machinery (Aymard et al. 2017). In this case, fill-in synthesis might promote translocation or NHEJ when cells enter S phase. Localized DNA synthesis might also manifest itself when a replication fork converges onto ssDNA breaks, leading to single-ended DSBs. Rescue of the replication fork can occur by HDR using the intact sister chromatid as a repair template. Under these conditions, resection tract lengths might be significantly shorter than we have observed upon AsiSI restriction enzyme cutting in NHEJ-deficient cells. If AsiSI cuts both sister chromatids (in S or G2) or if no sister chromatid is available (G1), reiterative engagement of the long-range resection machinery might result in hyperresection (Paiano et al. 2020). In contrast, much less homology

and shorter resection tracts might be required if the sister chromatid can be rapidly engaged. Under such conditions, localized DNA synthesis might prevent the formation of long 3' overhangs susceptible to mutagenic single-strand annealing (Ochs et al. 2016), or even recreate DNA ends that are competent for NHEJ. This could potentially explain why Pola inhibitors reduce radial chromosome fusions in BRCA1-deficient cells treated with PARPi (Mirman et al. 2018). Since radial fusions require LIG4-dependent NHEJ (Bunting et al. 2010), it is possible that Pola-mediated synthesis is necessary to generate compatible DNA ends during S phase. In addition to PARPi, topoisomerase I poisons produce single-ended DSBs, accumulation of which is lethal to HDR mutant cells. A recent study showed that resection in ATM-mutant cells was inefficient, causing these cells to be subject to radial chromosome fusions upon treatment with topoisomerase I poisons (Balmus et al. 2019). Strikingly, this toxicity could be suppressed by impairing LIG4-mediated NHEJ but not 53BP1 (Balmus et al. 2019). It is possible that 53BP1-independent Pola fill-in may counteract inefficient resection associated with ATM deficiency, thereby promoting toxic NHEJ. In conclusion, fill-in synthesis may be used at one-ended DSBs either to prevent mutagenic single-strand annealing or to salvage NHEJ postresection.

Recent work suggested a compelling model in which 53BP1 exerts its influence over resection through initiation of fill-in synthesis rather than (or in addition to) solely blocking exonuclease activity (Mirman et al. 2018). While inhibiting DNA synthesis in 53BP1-proficient cells robustly increased exonuclease activity on DSB ends, it did not fully recapitulate the hyperresection observed after loss of 53BP1 alone, indicating that other aspects of 53BP1 function, such as end protection, may be more critical to preventing hyperresected DSBs. Consistently, using a novel EXO1 inhibitor, we revealed that EXO1 is solely responsible for long-range resection in *Lig4*-null cells, while DNA2 plays an additional role in the hyperresection of *Lig4/53bp1*-deficient cells.

A recent study demonstrated that CST-Pola can initiate synthesis in a 53BP1- and Shieldin-dependent manner at the termini, but not at the center, of complementary 3' protruding ends, nor does it act at 5' ssDNA protrusions (Schimmel et al. 2021). Our data suggest that, for a subset of DSB intermediates, POLA-mediated fill-in can be achieved even in the absence of 53BP1/Shieldin. This raises the important and unanswered question of how POLA is recruited to DSBs in the absence of 53BP1/Shieldin. As CST can directly bind ssDNA (Rice and Skordalakes 2016), CST may recruit Pola directly onto resected DSBs. Alternatively, Pola may be recruited independently of CST through its interaction with RPA. Notably, RPA has been shown to interact with Pola *in vitro* and can stimulate primase activity (Dornreiter et al. 1992; Braun et al. 1997; Maga et al. 2001). While the physiological role of Pola/primase-mediated fill-in at DSBs remains unclear, our data suggest that the predominant mechanism by which 53BP1 limits resection is through 5' end blockade.

Materials and methods

Cell lines and cell culture

WT and *Lig4*^{-/-} Abelson-transformed murine pre-B cells expressing AsiSI-ER were generated as previously described (Canela et al. 2016). For G0/G1 cell cycle arrest, asynchronously cycling cells were treated with 3 μ M imatinib/STI (Selleckchem S2475) for 48 h at 1×10^6 cells/mL. To induce AsiSI-ER cutting, cells were treated with 3 μ g/mL doxycycline for 24 h, followed by 1 μ M 4-hydroxytamoxifen for an additional 18 h, unless otherwise noted. Cells were grown in DMEM supplemented with 5% FBS, 1% pen/strep, 1% glutamine, 1% sodium pyruvate, 1% nonessential amino acids, and 55 μ M β -mercaptoethanol. For G2 cell cycle arrests, asynchronously growing cells were treated with 10 μ M CDK1 inhibitor RO3306 (Sigma SML0569) for 36 h prior to AsiSI cutting. Aphidicolin (Sigma A0781), hydroxyurea (Sigma H8627), and DNA polymerase α inhibitors adarotene (MCE HY-14808) and CD437 (Sigma 178496) were added concurrently with 4-hydroxytamoxifen treatment at the doses indicated in the text. For exonuclease inhibition experiments, EXO1 inhibitor (C73) and DNA2 inhibitor (NCI repository NSC-105808) were added concurrently with 4-hydroxytamoxifen at 20 μ M and 2 μ M, respectively.

Generation of *Lig4*^{-/-}53bp1^{-/-} and *Lig4*^{-/-}Rev7^{-/-} AsiSI-ER cells

Lig4^{-/-}53bp1^{-/-} AsiSI-ER or *Lig4*^{-/-}Rev7^{-/-} cells were generated by inactivating 53bp1 or Rev7 in *Lig4*^{-/-} AsiSI-ER cells used in this study that were previously described (Canela et al. 2016). Briefly, 10 million *Lig4*^{-/-} AsiSI-ER cells, pretreated with 2 mg/mL doxycycline for 24 h, were nucleofected with 6 μ g of pX330-g53bp1 (53bp1 gRNA) or pX330-gRev7 (Rev7 gRNA) and 2 μ g of pKLV-hCD2 (human CD2) DNA in Amaxa 4D-Nucleofector X unit in solution SG using the pulse code CM-147 (Lonza). Twenty-four hours after nucleofection, hCD2-positive cells were purified by sequential staining with biotin-conjugated anti-hCD2 antibody and antibiotin antibody-conjugated streptavidin magnetic microbeads and selection on MS columns (Miltenyi). The selected cells were allowed to recover for 7–10 d before subcloning by limited dilution. Protein extract from single clones were subject to Western blot analysis to verify the loss of REV7 protein.

RPA foci quantification

For immunofluorescence assays, WT and *Brca1* ^{Δ 11/ Δ 11}53bp1^{-/-} MEFs (Bunting et al. 2010) were grown on 18-mm \times 18-mm glass coverslips. Cells were incubated with 10 μ M EdU (Invitrogen) for 30 min, washed, and treated with 10 Gy of γ -irradiation (137Cs Mark 1 irradiator, JL Shepherd). Following irradiation, cells were allowed to recover for 3 h. Cells were then pre-extracted as previously described (Zong et al. 2019) and fixed with 4% paraformaldehyde/1 \times PBS. After washing cells with 1 \times PBS, RPA antibody (1:2000; Cell Signaling 2208) was incubated for 2 h at 37°C. Fluorochrome-conjugated secondary antibodies (Invitrogen) were used for detection. Click-iT chemistry was performed as per the manufacturer's instructions (Thermo Fisher Scientific), and DNA was stained with DAPI (Thermo Fisher Scientific). Images were captured at 40 \times magnification on a Lionheart LX automated microscope (BioTek Instruments, Inc.). Quantification of EdU-positive (i.e., S-phase cells) nuclear RPA foci was performed using the Gen5 spot analysis software (BioTek). DNA2 inhibitor (2 μ M), EXO1 inhibitor/C73 (20 μ M), or both inhibitors were added 2 h before irradiation and were kept until pre-extraction.

Flow cytometry and Western blot

Cells were fixed in 1% formaldehyde for 10 min at room temperature, followed by saponin permeabilization for 10 min on ice. For DNA damage quantification, cells were washed in FACS buffer (1 \times PBS, 1% BSA) and incubated with anti-phospho-KAP1 antibody (diluted 1:100 in FACS buffer) (Thermo Fisher A300-767A) for 1 h at room temperature. Cells were washed three times in FACS buffer and incubated with antirabbit AF647 secondary antibody for 30 min at room temperature. Cells were washed three times in FACS buffer and analyzed on FACSCanto. For cell cycle profiling, 10 μ M EdU (Thermo Fisher A1004) was added to cells 30 min before fixation. AF488 Click-iT reaction was performed per the manufacturer's protocol (Thermo Fisher C10425), and 1 μ g/mL DAPI was added directly before FACS analysis. For Western blotting, cells were lysed in 50 mM Tris-HCl (pH 7.5), 200 mM NaCl, 5% Tween, 0.5% NP-40, 2 mM PMSF, 2 mM β -glycerophosphate disodium salt hydrate, and 1 tablet of cComplete mini protease inhibitor cocktail (Roche 11836153001). After transfer, membranes were incubated with 1:1000 anti-53BP1 antibody (Novus NB100-305) or 1:1000 anti-REV7 antibody (Santa Cruz Biotechnology sc-135977) overnight at 4°C.

Virtual screening of EXO1 inhibitor

We predicted druggable sites on the X-ray structure of hEXO1 (PDB ID 5v08) using an in-house-developed Druggable Site Prediction by FDA-approved drugs (DSP) methodology. A diverse subset of 100 FDA-approved drug molecules were docked around the protein surface and predicted the optimal binding site on the protein surface. Virtual high-throughput screening (vHTS) for molecules binding to the predicted druggable target site on EXO1 was carried out using an in-house-developed multiple-stage full-coverage (MSFC-VS) algorithm to screen an in silico a library of 260,071 compounds from the National Cancer Institute Developmental Therapeutics Program (NCI DTP) library. Metal coordination constraint was applied to adopt the ligand atom to chelate the metal coordination site of the target. The top 115 hit compounds based on the docking scores were assayed for their inhibition of hEXO1 by the nuclease assay.

EXO1 nuclease assay

Recombinant EXO1 was expressed in insect cells and purified following the protocol as previously described (Zhang et al. 2005). To conduct FRET-based EXO1 inhibitor screening, the FRET-DNA substrate (200 nM) was incubated with buffer only (blank), EXO1 (0.25 nM) in the absence or presence of 1% DMSO, or a candidate EXO1 inhibitor (10 μ M) in a reaction buffer (50 mM HEPES-KOH at pH 7.5, 45 mM KCl, 5 mM MgCl₂, 1 mM DTT, 100 μ g/mL BSA). The reaction was carried out in a 384-well black plate at 37°C, and the fluorescence signal was read by a Biotek microplate reader at 10 min. The RFU in the blank was subtracted from that in each EXO1 reaction. The relative activity was calculated by setting the subtracted RFU in the reaction with EXO1 and 1% DMSO (control) as 100% and comparing the subtracted RFU value in a reaction in the presence of a candidate EXO1 inhibitor with the control RFU.

To assay EXO1 activity using the ³²P-based DNA substrate, ³²P-DNA substrate (40 nM) was incubated with buffer only or EXO1 (0.25 nM) in the absence or presence of 1% DMSO or 10 μ M C73 in a reaction buffer (50 mM HEPES-KOH at pH 7.5, 45 mM KCl, 5 mM MgCl₂, 1 mM DTT, 100 μ g/mL BSA). The reaction was carried out for 10 min at 37°C, and DNA substrate and product were resolved in 15% denaturing PAGE and visualized by autoradiography.

END-seq

END-seq was performed as previously described (Canela et al. 2016; Paiano et al. 2020). For one sequencing library, 40 million live pre-B cells were embedded into a 0.75% agarose plug and immediately treated with Proteinase K for 1 h at 50°C then for 7 h at 37°C, followed by RNase for 1 h at 37°C. DNA double-strand break ends were blunted with exonuclease VII (NEB) for 1 h at 37°C and exonuclease T (NEB) for 45 min at 24°C. Biotin-adaptor ligations, agarose plug melting, DNA sonication, streptavidin capture, and library preparation were performed as previously described (Canela et al. 2016; Tubbs et al. 2018; Paiano et al. 2020; Wu et al. 2021).

ChIP-seq and single-strand DNA sequencing (SSDS)

MRE11 ChIP-seq (Paiano et al. 2020) and RPA single-strand DNA sequencing (Khil et al. 2012; Tubbs et al. 2018) were performed as previously described. Twenty million pre-B cells were used per library for ChIP-seq and SSDS. Cells were fixed in 1% formaldehyde in culture media (Sigma F1635) for 10 min at 37°C, quenched with 125 mM glycine (Sigma), washed twice with cold 1× PBS, snap-frozen on dry ice, and stored at -80°C until sonication and ChIP. Sonication, immunoprecipitation, and library preparation were performed as previously detailed (Tubbs et al. 2018; Paiano et al. 2020). Prior to all immunoprecipitations, sheared chromatin was precleared with 40 μL of Dynabeads Protein A (Thermo Fisher) for 30 min at 4°C. For MRE11 ChIP-seq, sheared chromatin was enriched with 4 μL of anti-MRE11 (Novus NB100-142) bound to Dynabeads Protein A overnight at 4°C. For RPA SSDS, sheared chromatin was enriched with 10 μg of anti-RPA32/RPA2 antibody (Abcam ab10359) on Dynabeads Protein A overnight at 4°C. During library preparation, kinetic enrichment of single-strand DNA was performed (Khil et al. 2012), thus sequencing only RPA-bound ssDNA, by heating sheared DNA fragments for 3 min at 95°C and allowing DNA to return to room temperature.

SAR-seq and in vitro SAR-seq

SAR-seq was performed as previously described (Wu et al. 2021) with 40 million pre-B cells used per library. EdU (20 μM; Thermo Fisher A1004) was added to cells concurrently with 4-OHT and kept in culture during the entire 18-h AsiSI cutting. To modify the SAR-seq protocol for DNA strand-specific sequencing (see Supplemental Fig. 1D; Wu et al. 2021), additional steps were taken prior to PCR library amplification. The streptavidin-captured, EdU-incorporated DNA fragments were washed in 1× SSC buffer followed by 10-min incubation with 0.15 M NaOH to denature DNA strands. Fragments were washed once with 0.1 M NaOH to fully remove non-EdU-incorporated DNA strands (i.e., those strands not bound to streptavidin-coated Dynabeads). EdU-containing ssDNA was then PCR-amplified and sequenced.

For in vitro SAR-seq, 20 million live pre-B cells were embedded into 0.75% agarose plugs digested with Proteinase K (50°C for 1 h, then 37°C for 7 h) per the END-seq protocol. They were then washed four times for 15 min each at room temperature by shaking with wash buffer (10 mM Tris-HCl at pH 8.0, 50 mM EDTA) and then four times for 15 min each at room temperature by shaking with EB (10 mM Tris-HCl at pH 8.0). They were then washed once for 15 min at room temperature by shaking in the appropriate 1× polymerase reaction buffer: NEBuffer 2 (B7002S) for DNA polymerase I and Klenow fragment 3' → 5' exo- or NEB T4 ligase buffer (B0202S) for T4 DNA polymerase. After washing, they were incubated with 1× appropriate reaction buffer, 10 mM EdU-dNTP mix (dATP, dCTP, dGTP, and EDU) and one of three

polymerases: DNA polymerase I (M0209S), T4 DNA polymerase (M0203L), or Klenow fragment 3' → 5' exo- (NEB), for 2 h. They were then washed four times for 15 min each at room temperature by shaking with EB and then twice for 15 min each at room temperature by shaking with 1× PBS before addition of biotin-azide click reaction (added in order immediately before reaction: 1× PBS, 3 mM copper sulfate, 50 μM biotin azide [Thermo Fisher B10184], 1× Click-iT additive [Thermo Fisher C10425]) for 2 h at room temperature with shaking. They were then washed four times for 15 min each at room temperature with shaking in wash buffer before being stored for no more than 1 wk at 4°C.

The agarose plugs were then washed four times in TE (10 mM Tris-HCl at pH 8.0, 1 mM EDTA) before being melted for 2 min at 70°C, cooled for 5 min at 43°C, and then incubated for 45 min at 43°C with 1.5 μL of β-agarase. The DNA in melted agarose was then incubated with 1 μL of 10% SDS and 4 μL of 20 mg/mL proteinase K for 15 min at 50°C. After that, the DNA was sonicated in a Covaris S220 series ultrasonicator at Cycle 1/duty 10%, intensity 175.0, cycles/burst 200, and 240 sec at 4°C–7°C. After sonication, the DNA was precipitated with ethanol and sodium acetate and then resuspended in EB before sequencing library preparation as previously described in the SAR-seq protocol (Wu et al. 2021).

Genome alignment

END-seq, SAR-seq, ChIP-seq, and RPA SSDS single-end reads were aligned to the mouse genome (GRCm38p2/mm10) using Bowtie v1.1.2 (PMID: 19261174) with parameters (-n 3 -k 1 -l 50) for END-seq and (-n 2 -m 1 -l 50) for others. All plots or analysis were done for the top 200 AsiSI sites determined by END-seq.

Resection quantification

To quantify the width of maximum resection endpoint, a sliding window containing 10 50-bp bins was used to start from the summit of each break, out to 5 kb on either side of the summit to detect the END-seq signal around the break summit. Maximum END-seq signal for 50-bp bins within 3~5 kb around the break summit was used as background. When more than half of the bins within this sliding window had an RPKM value equal to or lower than the background, then the last bin within the window that had a detectable signal over background was regarded as the maximum resection endpoint from the break summit.

Resection ratio is calculated using read counts at 115 bp~3 kb around the break summit divided by total reads within 3 kb around the break summit.

Data visualization

Alignment files were generated and sorted using SAMtools (Li et al. 2009) and converted to bedgraph files using bedtools genomcov (Quinlan and Hall 2010) following by bedGraphToBigWig to make a bigwig file (Kent et al. 2010). Visualization of genomic profiles was done by the UCSC browser (Kent et al. 2002) and normalized to present RPM.

Heat maps were produced using the R package pheatmap.

Statistical analysis

Statistical analysis was performed using R version 4.0.4 (<http://www.r-project.org>). The statistical test used in the box plot for resection quantification, RPA/SAR-seq intensity, is an unpaired *t* test.

Data availability

END-seq, RPA SSSDs, SAR-seq, in vitro EDU-seq, and ChIP-seq data have been deposited in the Gene Expression Omnibus (GEO) database under the accession number GSE181670.

Competing interest statement

The authors declare no competing interests.

Acknowledgments

We thank Dali Zong for comments on the manuscript; the CCR genomics core for help with sequencing. B.P.S.'s laboratory is supported by National Institutes of Health (NIH) R01 grants AI047829 and AI074953. B.S.'s laboratory is supported by National Cancer Institute/NIH grants R01CA085344 and R50CA211397. A.N.'s laboratory is supported by the Intramural Research Program of the NIH, an Ellison Medical Foundation Senior Scholar in Aging award (AG-SS-2633-11), Department of Defense awards (W81XWH-16-1-599 and W81XWH-19-1-0652), the Alex's Lemonade Stand Foundation Award, and an NIH Intramural FLEX Award.

Author contributions: J.P., N.Z., and W.W. designed most of the experiments. J.P. and N.Z. performed END-seq and SAR-seq. R.P. performed RPA SSSDs. B.-R.C. generated the cell lines. W.W. performed and interpreted the bioinformatic analyses. C.W. purified exonuclease 1 protein and did biochemical, cellular biological assays, and kinetic analysis to determine the IC50 of the inhibitors. H.L. did virtual screening of the compound library to suggest the candidate compounds for biochemical and cellular biological assays. L.Z. developed the fluorescence-based assay system and supervised the biochemical and cellular biological assays and kinetic analysis. B.S., B.P.S., and A.N. supervised the project. J.P. and A.N. wrote the manuscript with feedback from all authors.

References

- Abdel-Samad R, Aouad P, Gali-Muhtasib H, Sweidan Z, Hmadi R, Kadara H, D'Andrea EL, Fucci A, Pisano C, Darwiche N. 2018. Mechanism of action of the atypical retinoid ST1926 in colorectal cancer: DNA damage and DNA polymerase α . *Am J Cancer Res* **8**: 39–55.
- Aymard F, Aguirrebengoa M, Guillou E, Javierre BM, Bugler B, Arnould C, Rocher V, Iacovoni JS, Biernacka A, Skrzypczak M, et al. 2017. Genome-wide mapping of long-range contacts unveils clustering of DNA double-strand breaks at damaged active genes. *Nat Struct Mol Biol* **24**: 353–361. doi:10.1038/nsmb.3387
- Balmus G, Pilger D, Coates J, Demir M, Sczaniecka-Clift M, Barros AC, Woods M, Fu B, Yang F, Chen E, et al. 2019. ATM orchestrates the DNA-damage response to counter toxic non-homologous end-joining at broken replication forks. *Nat Commun* **10**: 87. doi:10.1038/s41467-018-07729-2
- Barazas M, Annunziato S, Pettitt SJ, de Krijger I, Ghezraoui H, Roobol SJ, Lutz C, Frankum J, Song FF, Brough R, et al. 2018. The CST complex mediates end protection at double-strand breaks and promotes PARP inhibitor sensitivity in BRCA1-deficient cells. *Cell Rep* **23**: 2107–2118. doi:10.1016/j.celrep.2018.04.046
- Bouwman P, Aly A, Escandell JM, Pieterse M, Bartkova J, van der Gulden H, Hiddingh S, Thanasoula M, Kulkarni A, Yang Q, et al. 2010. 53BP1 loss rescues BRCA1 deficiency and is associated with triple-negative and BRCA-mutated breast cancers. *Nat Struct Mol Biol* **17**: 688–695. doi:10.1038/nsmb.1831
- Braun KA, Lao Y, He Z, Ingles CJ, Wold MS. 1997. Role of protein-protein interactions in the function of replication protein A (RPA): RPA modulates the activity of DNA polymerase α by multiple mechanisms. *Biochemistry* **36**: 8443–8454. doi:10.1021/bi970473r
- Bunting SF, Call n E, Wong N, Chen HT, Polato F, Gunn A, Bothmer A, Feldhahn N, Fernandez-Capetillo O, Cao L, et al. 2010. 53BP1 inhibits homologous recombination in Brca1-deficient cells by blocking resection of DNA breaks. *Cell* **141**: 243–254. doi:10.1016/j.cell.2010.03.012
- Callen E, Zong D, Wu W, Wong N, Stanlie A, Ishikawa M, Pavani R, Dumitrache LC, Byrum AK, Mendez-Dorantes C, et al. 2020. 53BP1 enforces distinct pre- and post-resection blocks on homologous recombination. *Mol Cell* **77**: 26–38.e7. doi:10.1016/j.molcel.2019.09.024
- Canela A, Sridharan S, Sciascia N, Tubbs A, Meltzer P, Sleckman BP, Nussenzweig A. 2016. DNA breaks and end resection measured genome-wide by end sequencing. *Mol Cell* **63**: 898–911. doi:10.1016/j.molcel.2016.06.034
- Cejka P, Cannavo E, Polaczek P, Masuda-Sasa T, Pokharel S, Campbell JL, Kowalczykowski SC. 2010. DNA end resection by Dna2-Sgs1-RPA and its stimulation by Top3-Rmi1 and Mre11-Rad50-Xrs2. *Nature* **467**: 112–116. doi:10.1038/nature09355
- Chapman JR, Barral P, Vannier JB, Borel V, Steger M, Tomas-Loba A, Sartori AA, Adams IR, Batista FD, Boulton SJ. 2013. RIF1 is essential for 53BP1-dependent nonhomologous end joining and suppression of DNA double-strand break resection. *Mol Cell* **49**: 858–871. doi:10.1016/j.molcel.2013.01.002
- Cincinelli R, Musso L, Guglielmi MB, La Porta I, Fucci A, Luca D'Andrea E, Cardile F, Colelli F, Signorino G, Darwiche N, et al. 2020. Novel adamantyl retinoid-related molecules with POLA1 inhibitory activity. *Bioorg Chem* **104**: 104253. doi:10.1016/j.bioorg.2020.104253
- Dev H, Chiang TW, Lescale C, de Krijger I, Martin AG, Pilger D, Coates J, Sczaniecka-Clift M, Wei W, Ostermaier M, et al. 2018. Shieldin complex promotes DNA end-joining and counters homologous recombination in BRCA1-null cells. *Nat Cell Biol* **20**: 954–965. doi:10.1038/s41556-018-0140-1
- Di Virgilio M, Callen E, Yamane A, Zhang W, Jankovic M, Gitlin AD, Feldhahn N, Resch W, Oliveira TY, Chait BT, et al. 2013. RIF1 prevents resection of DNA breaks and promotes immunoglobulin class switching. *Science* **339**: 711–715. doi:10.1126/science.1230624
- Domreiter I, Erdile LF, Gilbert IU, von Winkler D, Kelly TJ, Fanning E. 1992. Interaction of DNA polymerase α -primase with cellular replication protein A and SV40 T antigen. *EMBO J* **11**: 769–776. doi:10.1002/j.1460-2075.1992.tb05110.x
- Escribano-D az C, Orthwein A, Fradet-Turcotte A, Xing M, Young JT, Tk c J, Cook MA, Rosebrock AP, Munro M, Canny MD, et al. 2013. A cell cycle-dependent regulatory circuit composed of 53BP1-RIF1 and BRCA1-CtIP controls DNA repair pathway choice. *Mol Cell* **49**: 872–883. doi:10.1016/j.molcel.2013.01.001
- Feng L, Fong KW, Wang J, Wang W, Chen J. 2013. RIF1 counteracts BRCA1-mediated end resection during DNA repair. *J Biol Chem* **288**: 11135–11143. doi:10.1074/jbc.M113.457440
- Ferretti LP, Lafranchi L, Sartori AA. 2013. Controlling DNA-end resection: a new task for CDKs. *Front Genet* **4**: 99. doi:10.3389/fgene.2013.00099
- Findlay S, Heath J, Luo VM, Malina A, Morin T, Coulombe Y, Djerir B, Li Z, Samiei A, Simo-Cheyrou E, et al. 2018.

- SHLD2/FAM35A co-operates with REV7 to coordinate DNA double-strand break repair pathway choice. *EMBO J* **37**: e100158. doi:10.15252/emboj.2018100158
- Gao S, Feng S, Ning S, Liu J, Zhao H, Xu Y, Shang J, Li K, Li Q, Guo R, et al. 2018. An OB-fold complex controls the repair pathways for DNA double-strand breaks. *Nat Commun* **9**: 3925. doi:10.1038/s41467-018-06407-7
- Ghezraoui H, Oliveira C, Becker JR, Bilham K, Moralli D, Anzilotti C, Fischer R, Deobagkar-Lele M, Sanchiz-Calvo M, Fueyo-Marcos E, et al. 2018. 53BP1 cooperation with the REV7-shieldin complex underpins DNA structure-specific NHEJ. *Nature* **560**: 122–127. doi:10.1038/s41586-018-0362-1
- Gupta R, Somyajit K, Narita T, Maskey E, Stanlie A, Kremer M, Typas D, Lammers M, Mailand N, Nussenzweig A, et al. 2018. DNA repair network analysis reveals Shieldin as a key regulator of NHEJ and PARP inhibitor sensitivity. *Cell* **173**: 972–988.e23. doi:10.1016/j.cell.2018.03.050
- Iacovoni JS, Caron P, Lassadi I, Nicolas E, Massip L, Trouche D, Legube G. 2010. High-resolution profiling of γ H2AX around DNA double strand breaks in the mammalian genome. *EMBO J* **29**: 1446–1457. doi:10.1038/emboj.2010.38
- Karanam K, Kafri R, Loewer A, Lahav G. 2012. Quantitative live cell imaging reveals a gradual shift between DNA repair mechanisms and a maximal use of HR in mid S phase. *Mol Cell* **47**: 320–329. doi:10.1016/j.molcel.2012.05.052
- Kent WJ, Sugnet CW, Furey TS, Roskin KM, Pringle TH, Zahler AM, Haussler D. 2002. The human genome browser at UCSC. *Genome Res* **12**: 996–1006. doi:10.1101/gr.229102
- Kent WJ, Zweig AS, Barber G, Hinrichs AS, Karolchik D. 2010. BigWig and BigBed: enabling browsing of large distributed datasets. *Bioinformatics* **26**: 2204–2207. doi:10.1093/bioinformatics/btq351
- Khil PP, Smagulova F, Brick KM, Camerini-Otero RD, Petukhova GV. 2012. Sensitive mapping of recombination hotspots using sequencing-based detection of ssDNA. *Genome Res* **22**: 957–965. doi:10.1101/gr.130583.111
- Li H, Handsaker B, Wysoker A, Fennell T, Ruan J, Homer N, Marth G, Abecasis G, Durbin R, 1000 Genome Project Data Processing Subgroup. 2009. The sequence alignment/map format and SAMtools. *Bioinformatics* **25**: 2078–2079. doi:10.1093/bioinformatics/btp352
- Maga G, Frouin I, Spadari S, Hübscher U. 2001. Replication protein A as a ‘fidelity clamp’ for DNA polymerase α . *J Biol Chem* **276**: 18235–18242. doi:10.1074/jbc.M009599200
- Mirman Z, de Lange T. 2020. 53BP1: a DSB escort. *Genes Dev* **34**: 7–23. doi:10.1101/gad.333237.119
- Mirman Z, Lottersberger F, Takai H, Kibe T, Gong Y, Takai K, Bianchi A, Zimmermann M, Durocher D, de Lange T. 2018. 53BP1-RIF1-shieldin counteracts DSB resection through CST- and Pola-dependent fill-in. *Nature* **560**: 112–116. doi:10.1038/s41586-018-0324-7
- Miyake Y, Nakamura M, Nabetani A, Shimamura S, Tamura M, Yonehara S, Saito M, Ishikawa F. 2009. RPA-like mammalian Ctc1-Stn1-Ten1 complex binds to single-stranded DNA and protects telomeres independently of the Pot1 pathway. *Mol Cell* **36**: 193–206. doi:10.1016/j.molcel.2009.08.009
- Noordermeer SM, Adam S, Setiaputra D, Barazas M, Pettitt SJ, Ling AK, Olivieri M, Álvarez-Quilón A, Moatti N, Zimmermann M, et al. 2018. The shieldin complex mediates 53BP1-dependent DNA repair. *Nature* **560**: 117–121. doi:10.1038/s41586-018-0340-7
- Ochs F, Somyajit K, Altmeyer M, Rask MB, Lukas J, Lukas C. 2016. 53BP1 fosters fidelity of homology-directed DNA repair. *Nat Struct Mol Biol* **23**: 714–721. doi:10.1038/nsmb.3251
- Paiano J, Wu W, Yamada S, Sciascia N, Callen E, Paola Cotrim A, Deshpande RA, Maman Y, Day A, Paull TT, et al. 2020. ATM and PRDM9 regulate SPO11-bound recombination intermediates during meiosis. *Nat Commun* **11**: 857. doi:10.1038/s41467-020-14654-w
- Quinlan AR, Hall IM. 2010. BEDTools: a flexible suite of utilities for comparing genomic features. *Bioinformatics* **26**: 841–842. doi:10.1093/bioinformatics/btq033
- Rice C, Skordalakes E. 2016. Structure and function of the telomeric CST complex. *Comput Struct Biotechnol J* **14**: 161–167. doi:10.1016/j.csbj.2016.04.002
- Schimmel J, Muñoz-Subirana N, Kool H, van Schendel R, Tijsterman M. 2021. Small tandem DNA duplications result from CST-guided Pol α -primase action at DNA break termini. *Nat Commun* **12**: 4843. doi:10.1038/s41467-021-25154-w
- Setiaputra D, Durocher D. 2019. Shieldin - the protector of DNA ends. *EMBO Rep* **20**: e47560. doi:10.15252/embr.201847560
- Sheaff R, Ilsley D, Kuchta R. 1991. Mechanism of DNA polymerase α inhibition by aphidicolin. *Biochemistry* **30**: 8590–8597. doi:10.1021/bi00099a014
- Soniati MM, Myler LR, Kuo HC, Paull TT, Finkelstein IJ. 2019. RPA phosphorylation inhibits DNA resection. *Mol Cell* **75**: 145–153.e5. doi:10.1016/j.molcel.2019.05.005
- Symington LS. 2016. Mechanism and regulation of DNA end resection in eukaryotes. *Crit Rev Biochem Mol Biol* **51**: 195–212. doi:10.3109/10409238.2016.1172552
- Tomida J, Takata KI, Bhetawal S, Person MD, Chao HP, Tang DG, Wood RD. 2018. FAM35A associates with REV7 and modulates DNA damage responses of normal and BRCA1-defective cells. *EMBO J* **37**: e99543. doi:10.15252/emboj.201899543
- Tubbs A, Sridharan S, van Wietmarschen N, Maman Y, Callen E, Stanlie A, Wu W, Wu X, Day A, Wong N, et al. 2018. Dual roles of poly(dA:dT) tracts in replication initiation and fork collapse. *Cell* **174**: 1127–1142.e19. doi:10.1016/j.cell.2018.07.011
- Wu W, Hill SE, Nathan WJ, Paiano J, Callen E, Wang D, Shinoda K, van Wietmarschen N, Colon-Mercado JM, Zong D, et al. 2021. Neuronal enhancers are hotspots for DNA single-strand break repair. *Nature* **593**: 440–444. doi:10.1038/s41586-021-03468-5
- Zhang Y, Yuan F, Presnell SR, Tian K, Gao Y, Tomkinson AE, Gu L, Li GM. 2005. Reconstitution of 5'-directed human mismatch repair in a purified system. *Cell* **122**: 693–705. doi:10.1016/j.cell.2005.06.027
- Zhao B, Rothenberg E, Ramsden DA, Lieber MR. 2020. The molecular basis and disease relevance of non-homologous DNA end joining. *Nat Rev Mol Cell Biol* **21**: 765–781. doi:10.1038/s41580-020-00297-8
- Zimmermann M, Lottersberger F, Buonomo SB, Sfeir A, de Lange T. 2013. 53BP1 regulates DSB repair using Rif1 to control 5' end resection. *Science* **339**: 700–704. doi:10.1126/science.1231573
- Zong D, Adam S, Wang Y, Sasanuma H, Callén E, Murga M, Day A, Kruhlak MJ, Wong N, Munro M, et al. 2019. BRCA1 haploinsufficiency is masked by RNF168-mediated chromatin ubiquitylation. *Mol Cell* **73**: 1267–1281.e7. doi:10.1016/j.molcel.2018.12.010